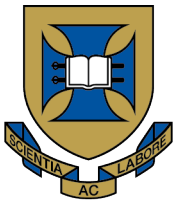

THE UNIVERSITY OF QUEENSLAND

AUSTRALIA

Design and Construction of a Ducted Rotor

by

Rory Gallagher

School of Information Technology and Electrical Engineering,
University of Queensland.

Submitted for the degree of
Bachelor of Engineering/Business Management
in the division of Mechatronics.

November 2015.

Rory Gallagher
42356051
6 Carlton Tce
Wynnum, QLD 4178

November 9, 2015

Prof Paul Strooper
Head of School
School of Information Technology and Electrical Engineering
The University of Queensland
St Lucia, QLD 4072

Dear Professor Strooper,

In accordance with the requirements of the degree of Bachelor of Engineering/Business Management in the division of Mechatronic Engineering, I present the following thesis entitled

"Design and Construction of a Ducted Rotor".

This work was performed under the supervision of Dr Paul Pounds. I declare that the work submitted in this thesis is my own, except as acknowledged in the text and footnotes, and has not been previously submitted for a degree at the University of Queensland or any other institution.

Yours sincerely,

Rory Gallagher

Abstract

The aim of this thesis project was to design and construct a ducted rotor so that the aerodynamic contribution of the duct would lead to an increase in performance, as well as providing shielding from the propellers to add to the safety of the design. The ducted rotor was designed on computer-aided Design (CAD) model and was tested successfully on CFD software. The design of the ducted rotor used an annular wing design at the leading edge of the duct to increase the thrust generated. The design implemented a slotted flap for boundary layer control to minimise flow separation as well as maximising the amount of laminar flow over the duct. Lastly, the design considered the benefit that the duct has for reducing the vortices forming at the tips of the propellers, by minimising clearance between the duct and the propeller tips. A physical model was constructed and tested, which showed a 19.8% decrease in power consumption when compared with a free propeller.

Contents

List of Figures

List of Tables

Nomenclature

Symbol	Description
UAV	Unmanned Aerial Vehicle
CFD	Computational Fluid Dynamics
CAD	Computer Aided Drawing
UQ	University of Queensland
ρ	Density
A	Area
V	Velocity
dp	Derivative
P	Pressure
g	Gravity
F	Force
m	Mass
a	Acceleration
Re	Reynold's Number
L	Lift Force
D	Drag Force
C_L	Coefficient of Lift
C_D	Coefficient of Drag
τ_w	Shear Stress
gsm	Grams per Square Meter

Chapter 1

Introduction

Micro Unmanned Aerial Vehicles (UAVs) offer significant benefits to both military and civilian applications. They offer the advantages of aerial vehicles without the burdening costs and impracticalities that are associated with larger, manned vehicles.

Ducted rotors add to the advantages associated with micro UAVs due to the aerodynamic contribution of the duct. When designed properly, ducted rotors are capable of having an increased overall efficiency compared with other rotor designs whilst also offering a safer vehicle to operate in close proximity to.

1.1 Aim of Thesis

The aim of the thesis was to improve the design of a ducted micro UAV by increasing efficiency and safety. The project analysed the aerodynamic performance of the duct through Computational Fluid Dynamics (CFD) and a physical test apparatus. Focus was placed on the leading edge of the duct, where an innovative inlet was designed to take advantage of the aerodynamic potential as fluid flows into the ducted rotor.

1.2 Summary of Achievements

Overall, the aims of the thesis were achieved and the innovative features in the design were shown to be effective. The stand-out achievements of this thesis were:

- A computer-aided Design (CAD) model was developed and tested successfully on CFD software
- A physical model was constructed and tested to verify the performance increase

- Improvements in performance were observed with the physical test model decreasing power consumption by 19.8%

1.3 Report Overview

The report will identify the aerodynamic features of a ducted rotor that are fundamental to the design. It will then explain the methods that were used to increase the performance of the design and why the chosen methods were appropriate. The final design will then be analysed and discussed as well as how it may still be improved.

Chapter 2

Background

UAVs are increasing in popularity worldwide and there is a growing demand for them to be more efficient and safe. Ducted rotors offer a way of achieving this through the aerodynamic contribution of the duct intake and the shielding provided by the body of the duct.

During the 20th century, there was a demand for ducted fan designs with vertical take-off and landing (VTOL) capabilities. In the 1950s, the Hiller Aircraft Corporation developed the Hiller VZ-1 Pawnee for the U.S. Army in an attempt to increase mobility of the troops on the battlefield (Figure 2.1). The ducted fan platform had contra-rotating rotors for lift and direction control was simplified by shifting the pilots body weight [1]. However, the VZ-1 Pawnee was unable to perform the desired capabilities as it could not achieve enough thrust to operate out of ground effect without annulling the pilots control using bodyweight.

Figure 2.1: Hiller VZ-1 Pawnee with pilot [1]

In the 1960s, the U.S. Navy ordered the X-22A aircraft from Bell for its vertical

and/or short take-off and landing (V/STOL) capabilities (Figure 2.2). The X-22A was a dual tandem ducted propeller aircraft that was capable of transitioning between hover and horizontal flight [2]. The success of the design showed that the ducted fan design was usable but the program was eventually cancelled.

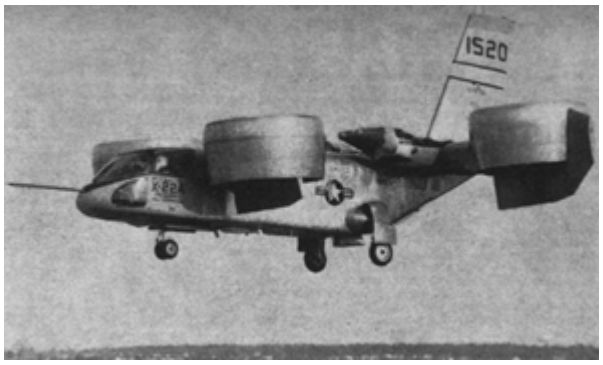

Figure 2.2: Bell X-22A [2]

More recently, an example of how the ducted rotors can be used safely for VTOL applications is the Martin Jetpack, which uses a twin ducted rotor design (Figure 2.3). With a flight time of 30 minutes the Martin Jetpack can reach speeds of 40 knots and has a ceiling of 3000 feet [3]. With safety a key consideration, Martin Jetpack Company has identified the advantages of using ducted fans:

"The use of ducted fans has a fundamental safety advantage over propellers and rotors. The tips of the blades are contained within the duct and are less of a safety hazard than exposed blades. This makes it safer for people near the aircraft, and reduces the risk of damage due to propellers or rotors coming into contact with objects."

Figure 2.3: Martin Jetpack with Ducted Rotors [3]

The Honeywell RQ-16A T-Hawk (Figure 2.4) is a Micro Air Vehicle (MAV) with

a ducted rotor design used by the U.S. Navy. With unmanned capabilities, it is a useful tool used by armed forces in combat zones for intelligence, surveillance and reconnaissance missions [4]. It shows that micro UAVs are effective with a ducted design.

Figure 2.4: Honeywell RQ-16A T-hawk [4]

In 2012, Robert Walker, an undergraduate student at the University of Queensland designed and constructed a MAV that expanded on the ducted rotor design by including an airfoil at the inlet of the duct (Figure 2.5). The design was capable of producing lift, however, it was concluded that this was developed due to the acceleration of flow through the duct and not the ring airfoil as anticipated [5]. Possible reasons for this were identified as flow separation at the inlet, skin friction or airfoil drag. This project will expand on the work completed by Walker, in an attempt to develop more lift through the ring airfoil design.

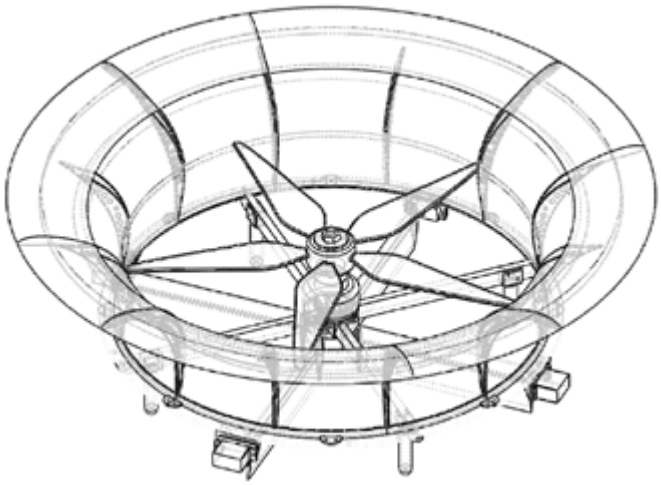

Figure 2.5: Robert Walker's MAV [5]

Chapter 3

Theory

The Following chapter will give a summary of the theory that is required for understanding the concepts mentioned later in this report.

3.1 Fluid Dynamics

A ducted fan is when the air flow is constrained within a ducted enclosure so that it must enter and leave the fan rotor in an axial direction [6]. Therefore, assuming the air to be incompressible, the continuity of flow through the duct can be assumed and expressed in Equation 3.1.

$$\rho_1 A_1 V_1 = \rho_2 A_2 V_2 \tag{3.1}$$

However, when the flow is accelerated through the duct due to the rotor, an increase in momentum is observed. Decreases in momentum can occur through losses, which mainly occur due to skin friction, flow separation, secondary flows and energy dissipation at the discharge [6]. To analyse the change in momentum through the rotor, the change in pressure must be considered [7]. Therefore, Eulers equation (Equation 3.2) is used as it relates the rate of change of momentum to force.

$$dp = -pV dV \tag{3.2}$$

When two points are considered along a streamline, Eulers equation can be integrated between the two points, resulting in Bernoullis equation (Equation 3.3). Both Eulers equation and Bernoullis equation are important because they are essentially Newtons second law (Equation 3.4) applied to fluid dynamics [7].

$$\frac{p_1}{\rho g} + \frac{v_1^2}{2g} = \frac{p_2}{\rho g} + \frac{v_2^2}{2g} \tag{3.3}$$

$$F = ma \tag{3.4}$$

The boundary layer is a region of flow retardation that represents the loss of fluid momentum through interactions between the fluid particles and a surface, which is referred to as skin friction [6]. The amount of skin friction is influenced by whether the flow is laminar or turbulent, where laminar flow creates less skin friction than turbulent flow [7]. This interaction observes a ratio of inertial forces to viscous forces in a fluid [11], also known as the Reynolds number (Equation 3.5). Due to this ratio, a boundary layer is created, where the velocity changes from zero at the surface and increases to the free stream velocity away from the surface (Figure 3.1).

$$Re = \frac{\rho \overline{U} l}{\mu} \tag{3.5}$$

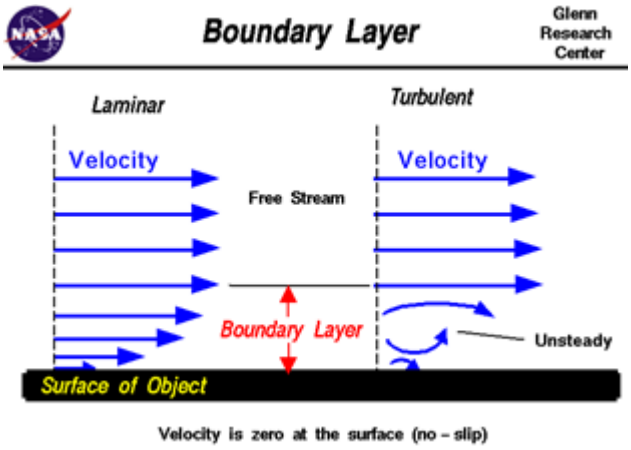

Figure 3.1: Boundary Layer next to a surface

3.2 Airfoil Forces

Airfoils are designed to provide a large normal force, N, whilst minimising the axial force, A, to the free stream velocity (Figure 3.2) [8]. The angle of attack is represented as α. Therefore the lift and drag forces, L and D, respectively, can be expressed (Equation 3.6 and 3.7) [7]. Furthermore, the dimensionless coefficients of lift and drag, C_L and C_D, can be represented with respect to the planform area of the airfoil, AP (Equation 8 and 9) [8]. These coefficients are used to compare different airfoil designs for given angles of attack and Reynolds numbers.

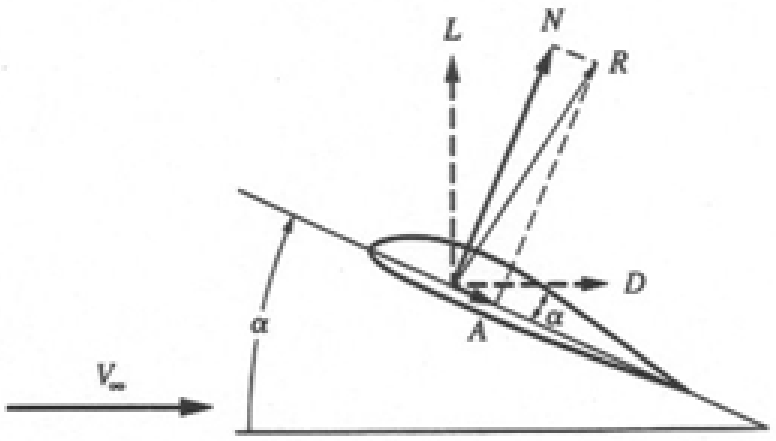

Figure 3.2: Forces acting on an Airfoil [7]

$$L = N\cos\alpha - A\sin\alpha \tag{3.6}$$

$$D = n\sin\alpha + A\cos\alpha \tag{3.7}$$

$$C_L = \frac{L}{\frac{1}{2}\rho V^2 A_P} \tag{3.8}$$

$$C_D = \frac{D}{\frac{1}{2}\rho V^2 A_P} \tag{3.9}$$

These aerodynamic forces that are exerted on an object in a moving fluid are a result of two main forces, pressure distribution on the surface of an object and shear stress, otherwise considered as the friction acting on the surface of the object [7]. These forces interact with the object and result in lift and drag forces being exerted.

The lift force exerted on an object is a result of the pressure distribution on the surface of the object, which is directly related to the fluid flow over the surface. The flow over an object separates from the flow below an object at the stagnation point, which is abbreviated as s.p. in Figure 3.3 [7].

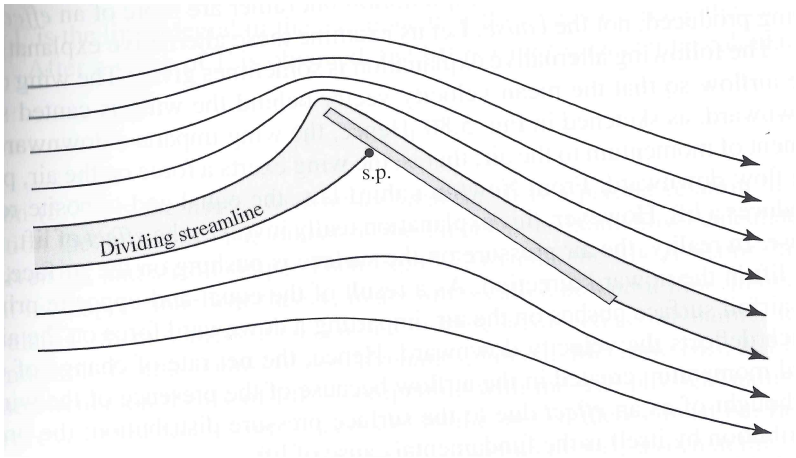

Figure 3.3: Flow Around an Object [7]

As the flow separates, a difference in the pressure distribution around the object is created, as shown in Figure 3.4

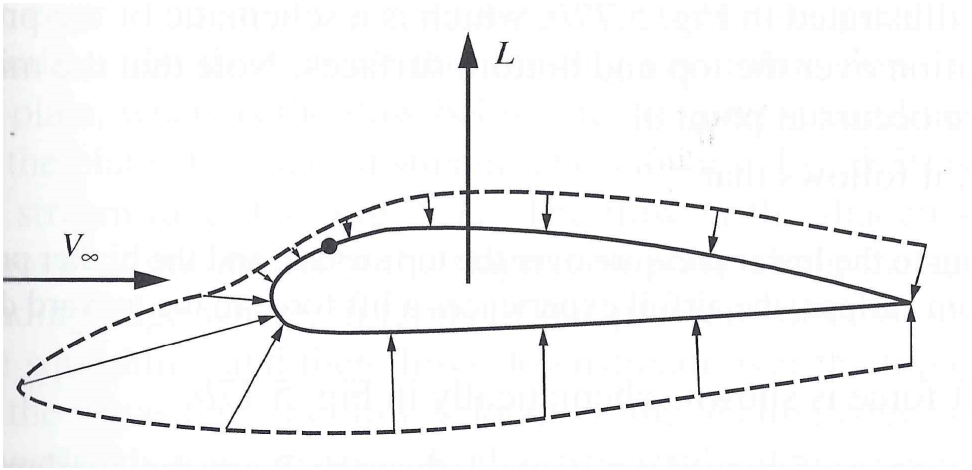

Figure 3.4: Pressure Distribution Around an Airfoil [7]

It is important to consider the flow over the top and bottom of the airfoil as separate stream tubes as shown in Figure 3.5. Stream tube A, which flows over the top of the airfoil, separates from stream tube B at the stagnation point. Due to the physical presence of the airfoil, as the flow from stream tube A flows over the airfoil, the stream tubes cross sectional area is reduced. This reduction in cross sectional flow area can be seen in Figure 3.3, where it is clearly seen that the streamlines come closer together. Due to the mass continuity of flow (Equation 3.1), the velocity of flow in stream tube A is increased. Therefore, from Bernoulli's equation (3.3), when the velocity increases, the static pressure decreases.

To consider the lower section of the flow, stream tube B, the stream tube's cross sectional area is not reduced as much, thus the velocity does not increase as much

and the static pressure does not decrease as much. Therefore, due to the Bernoulli effect the pressure over the top of the airfoil is less than the pressure below the airfoil. This pressure difference leads to a lift force being applied to the airfoil in an upwards direction. This force is a result of the fundamental laws of mass conservation and Newton's second law [7].

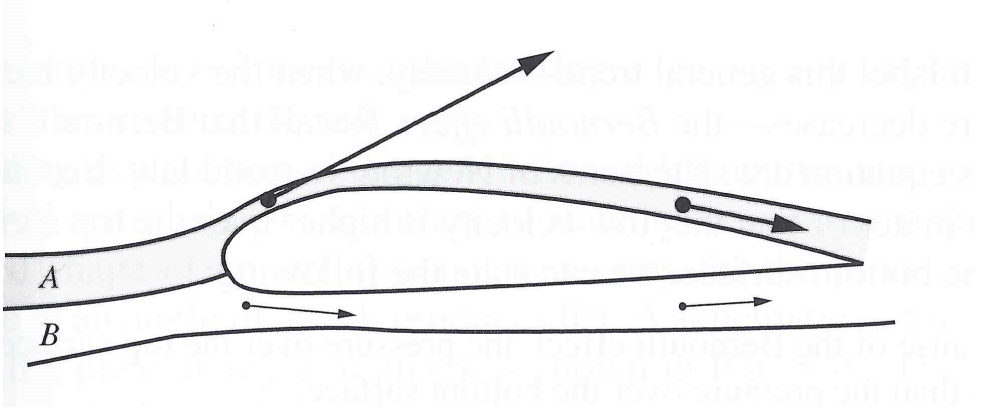

Figure 3.5: Stream Tubes [7]

The drag force exerted on an object is due to skin friction, pressure drag due to separation and induced drag [7].

Skin friction drag is due to the shear stress on the objects surface, which is due to the presence of friction in the flow at the objects surface. The shear stress acting on the surface of the object can be given by Equation 3.10 [7].

$$\tau_w = \mu \left(\frac{dV}{dY} \right) \tag{3.10}$$

The shear stress is dependant on whether the flow is laminar or turbulent. The laminar shear stress is less than the turbulent shear stress [7]. Therefore, laminar flow produces less skin friction drag.

As the fluid flows over the upper surface of an airfoil, the pressure decreases dramatically. However, as the flow continues to move further downstream over the airfoil, the pressure gradually increases. If the rate of pressure increase is too high, the flow will seperate. This gradual increase in pressure is why the airfoil shapes are necessary. Turbulent boundary layers have been shown to reduce flow seperation [7]. Therefore, flow seperation drag can be reduced by establishing a turbulant boundary layer. Flow separation has two major consequences on the performance of an object in a moving fluid, including; loss of lift and a major increase in drag, which is caused by pressure drag due to seperation [7].

3.3 Duct Leading Edge

The leading edge of a duct is capable of generating extra thrust due to the pressure distribution over its surface. As shown in Figure 3.6, the flow converges on the propeller, which is due to the momentum increase as well as the continuity of flow. However, due to the physical presence of the duct, the flow that is caught on the outside of the leading edge of the duct flows back around the leading edge into the flow due to the suction force created by the propeller. This suction force creates a pressure distribution around the leading edge as the fluid accelerates around the edge, resulting in extra thrust at this location [9].

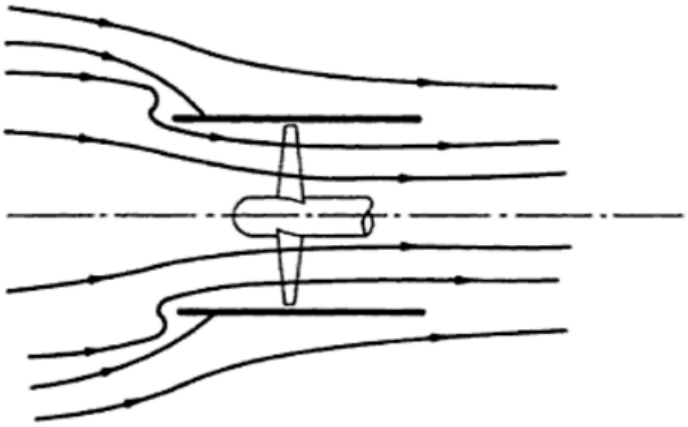

Figure 3.6: Straight Edge Duct [9]

However, when a fluid flows into a duct, if the inlet was straight, there would be flow separation at the leading edge of the duct. To avoid this flow separation, the mean camber line at the leading edge is curved outwards, creating a lip radius at the inlet [9].

Experimentation has shown that as the lip radius increases, the thrust generated increases. However, previous research has shown that the benefits of increasing the radius are diminished as the drag due to skin friction and the weight of the extra material increase [9].

3.4 Duct Dimensions

CFD testing for a ducted rotor UAV shows that the optimal dimensions of the duct consists of a design where the length is 50% of the throat diameter and the contraction of the design is 10 [10]. This shorter design is further backed up by evidence which shows that total thrust decreases sharply with an increase in the duct

length, where the rate of decrease is sharper for ducts that have high contraction angles [11].

3.5 Propeller

The rotor design within a duct varies significantly to rotor designs that arent confined within a duct, as there are different secondary flows at play. When a rotor is not confined within a duct, the higher pressure below the airfoil tends towards the lower pressure at the extreme end of the blade, causing secondary flow vortices at the tips, which in turn creates losses within the system [6]. Within a duct, the vortex that forms at the blade tip flows in a direction that is opposite to the flow through the duct and it is also limited by the physical wall of the duct. For this reason, the secondary flow is restricted, minimising any losses through secondary flows [6]. Evidence also shows that decreasing the blade tip clearance between the duct and blade can improve efficiency [10]. This implies that a ducted rotor should be as tight fitting as possible within the duct. As a result, the diameter of the duct will directly interact with the span of the rotor.

The performance and design of a duct cannot be considered in isolation of the rotor, due to the crucial interactions that they have with each other [6]. As a result, it is important to find the optimal efficiency operating point between the resistance of the duct and the rotor characteristic for given rotational speeds when total pressure and volumetric flow rates are considered (Figure 3.7). This operating point identifies the flow rate where the maximum pressure is obtained for a given rotor within a duct design [6], indicating that the design should be based around the operating point. This implies that for each duct design, a unique rotor with the required rotational velocities and flow rates should be used.

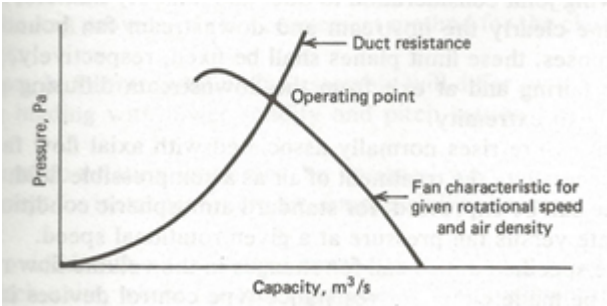

Figure 3.7: Matching of fan and duct system [6]

3.6 Boundary Layer Control

Slotted flaps, which are often referred to as high lift devices, are attached at the leading or trailing edge of an airfoil, which increases C_L and reduces the stall angle α [12]. The stall angle is the angle of attack at which stalling occurs at a particular speed. For this reason, slotted flaps increase lift at lower speeds. The optimal slotted flap position relies on the fact that there is minimal impact from the boundary layer of the other flap [13]. Furthermore, to optimise the slotted flap design of the airfoil, a two dimensional analysis has shown that having the appropriate gap between the slotted flaps is vital, which has been shown to change with different Reynolds numbers [13].
Separation can occur on high lift flaps. Fixed by having high pressure from below led through a converging channel to the lower pressure above. This helps overcome the strong adverse pressure gradients where there is flow separation and stall.

3.7 Material Properties

Each type of material has a different surface roughness, which affects the skin friction in fluid flow, where increasing surface roughness increases skin friction [14]. Furthermore, for micro UAV design, the overall weight should be reduced and stiffness and strength maximised. Therefore, material selection should consider the properties of multiple materials (Table 3.1).

Table 3.1: Material Properties

	PLA	Aluminium	Carbon Fibre
Density (g/cm^3)	1.2	2.79	1.6
Young's Modulus (GPa)	3.8	73.1	70

Chapter 4

Duct Design

This chapter will describe the key features for the ducted rotor and how the final design was achieved. The final CAD model of the ducted rotor is shown in Figure 4.1

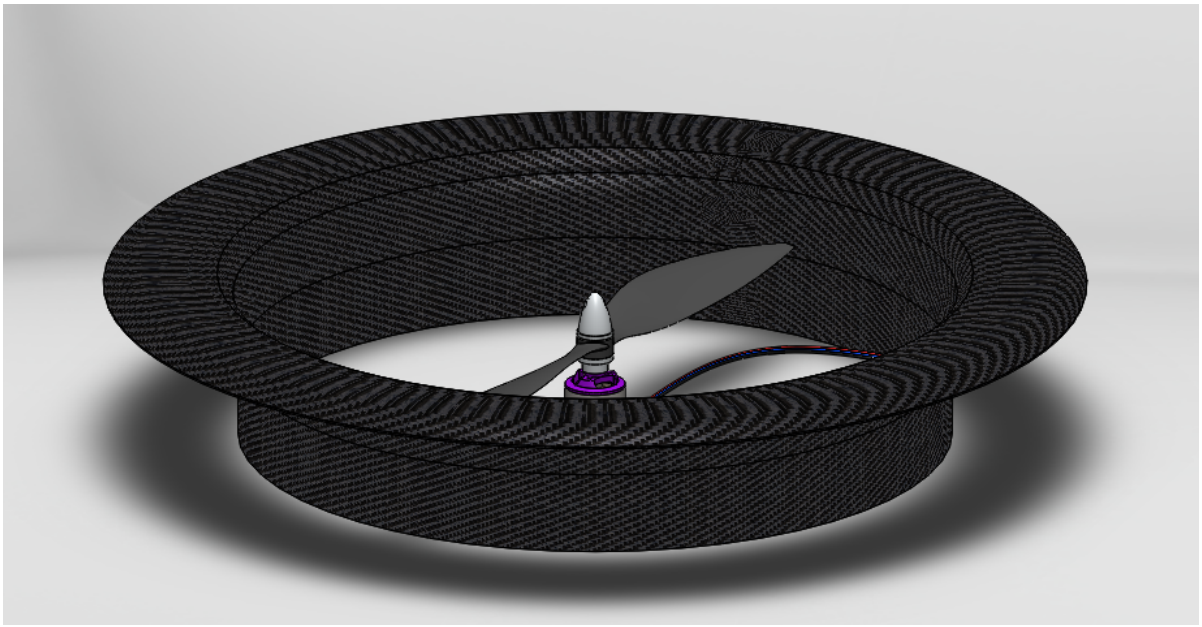

Figure 4.1: CAD view of the Ducted Rotor

4.1 Inlet Design

The design of the inlet had to consider the theory mentioned in Section 3.3 in order for the flow to not separate and to increase the thrust. The airfoil design at the leading edge, as highlighted in Figure 4.2 will be referred to as the annular wing.

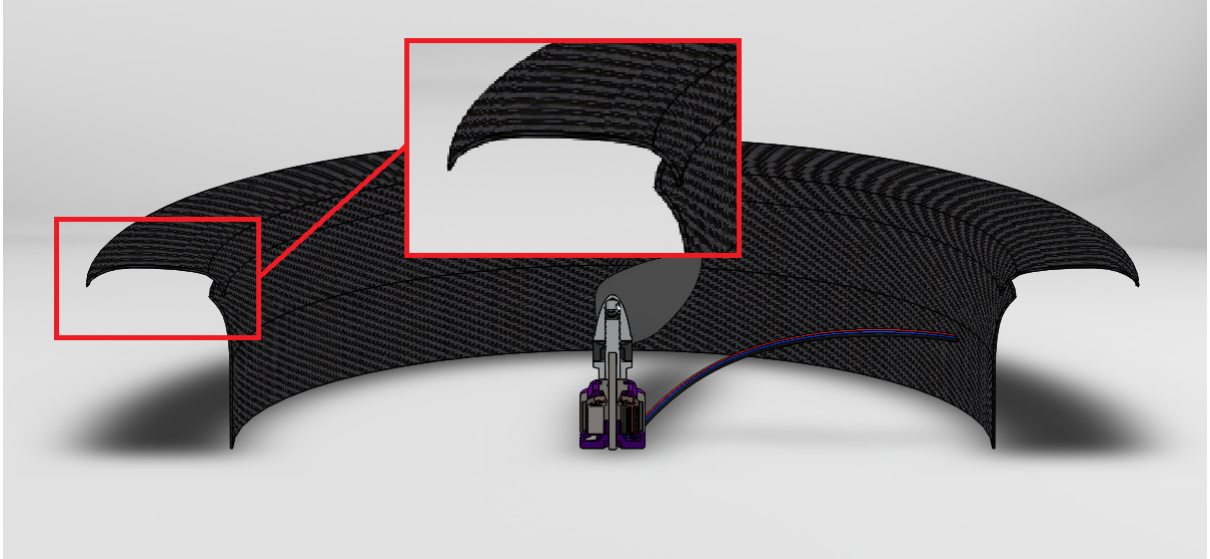

Figure 4.2: Highlight of Annular Wing on CAD Model Cross-Section

The annular wing was initially analysed with an upper and lower surface. However, as shown in Section 3.3, the upper surface of the leading edge is considered to be the more critical surface. Therefore, it was decided that the lower surface of the annular wing would not be added to the design as the benefits were outweighed by the construction complexity and extra weight.

As shown by Equation 3.8, the lift forces are increased as the planform area increases. Therefore, the chord length of the annular wing was considered to have an impact on the performance. Furthermore, as mentioned in Section 3.3, the camber of the leading edge of the duct influences the flow separation, giving reason to consider the camber of the annular wing in the design.

4.1.1 Camber of Annular Wing

The upper camber at the leading edge of the annular wing is critical in reducing flow separation as the fluid flowed over the top of the leading edge into the duct [9]. For this reason, multiple designs were analysed in ANSYS CFX (As shown in Figures 4.3 4.4 4.5). This was then used to determine a suitable upper camber that allowed the fluid to flow over the annular wing without flow separation.

Due to the fact that turbulent structures cannot be handled well by CFD simulations by most available computers [15], it can be difficult to get accurate numerical CFD results when the flow has separated. Therefore, it was determined that visually inspecting the flow from the simulated results for each iteration of upper camber would be a suitable method. For each design modelled on CFD, the flow over the

airfoil was visually inspected for flow separation.

Figures 4.3, 4.4 and 4.5 compare the designs with varying amounts of camber on the annular wing, which results in varying amount of flow separation. As can be seen, the design with an increased amount of camber has minimal flow separation as the fluid moves over the leading edge. This method proved to be effective in choosing a design with the correct camber.

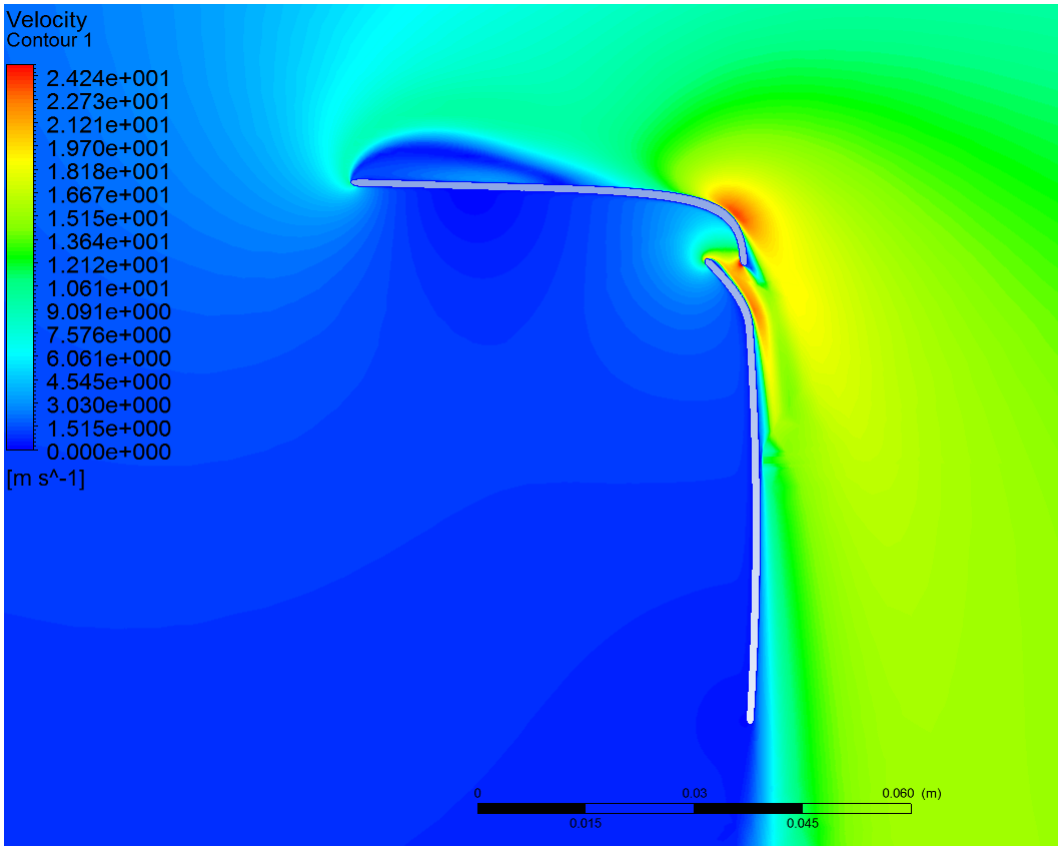

Figure 4.3: Cross Section View of Annular Wing with Minimal Camber and High amount of Flow Separation

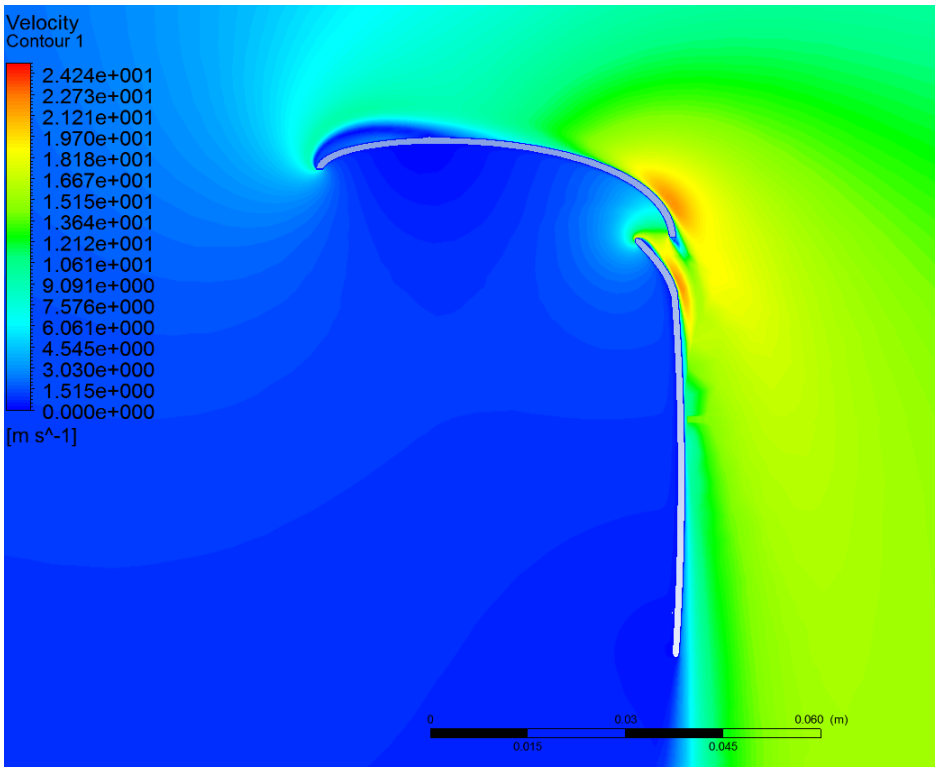

Figure 4.4: Cross Section View of Annular Wing with Moderate Camber and Moderate amount of Flow Separation

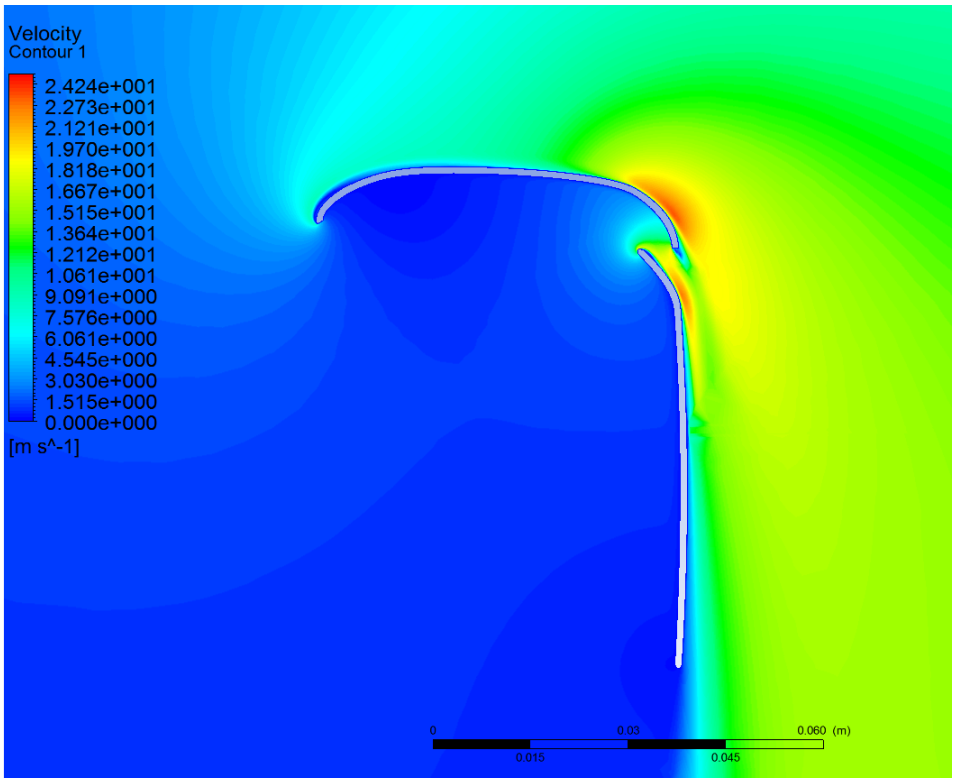

Figure 4.5: Cross Section View of Annular Wing with Increased Camber and Minimal amount of Flow Separation

4.1.2 Length of Annular Wing

The chord length of the annular wing was also considered in the design process, as a larger surface area results in a greater amount of thrust [9]. However, as the area increases you get diminishing returns due to the adverse affects of skin friction, as well as the added weight impede on the performance.

To determine the optimal area of the wing, the chord length was increased by increments of 10 mm and each design was tested in CFD simulations. The simulations considered the surface roughness of carbon fibre in the simulations.

The results from the analysis are shown in Figure 4.6, where it can be seen that the benefits from each incremental increase diminish. The thrust values represent that forces that are developed on the surface of the shroud and annular wing only. From these results, a final chord length of 55 mm was chosen.

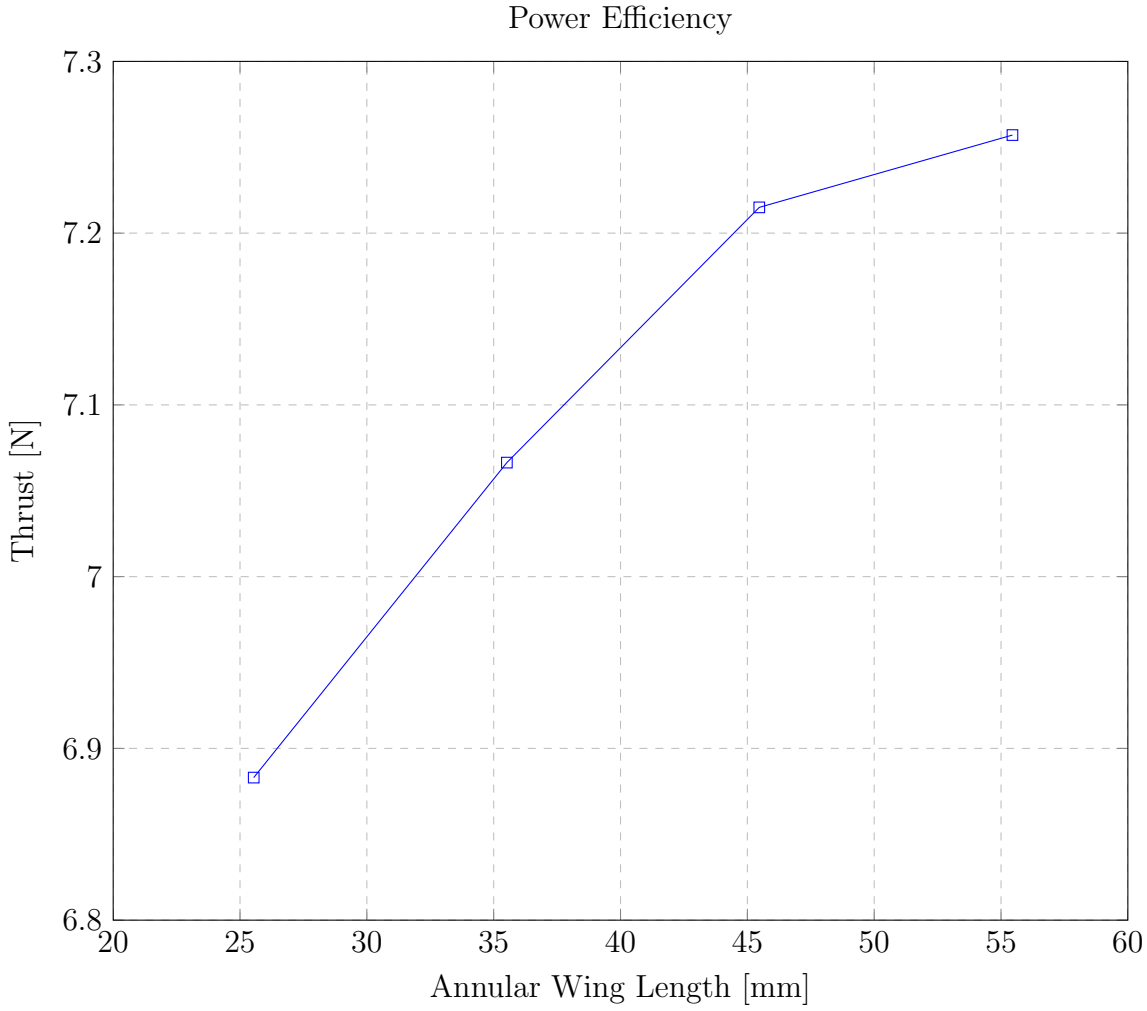

Figure 4.6: Diminishing Returns as Annular Ring Increases in Length

4.1.3 Earlier Annular Wing Considerations

It should be mentioned that based on previous studies, it was considered that the flow over the lower surface of the wing may improve performance [5]. To test this method, an annular wing with a full airfoil was modelled in CFD, where flow separation was unlikely. The thrust results were compared and it showed that there was minimal difference in results when the slot between the duct and the wing was closed. This showed that the upper surface of the annular wing is the most critical. This coincides with the theory mentioned in Section 3.3.

Table 4.1: Performance Difference with Flow Over Lower Surface of Annular Wing

Unjoined Duct $[N]$	Joined Duct $[N]$	Percentage Difference [%]
8.59	8.56	0.27

4.1.4 Boundary layer Control

As described by Walker [5], the benefits of having a slot around the inlet was recognised when the flow was susceptible to flow separation and was thus implemented during this analysis.

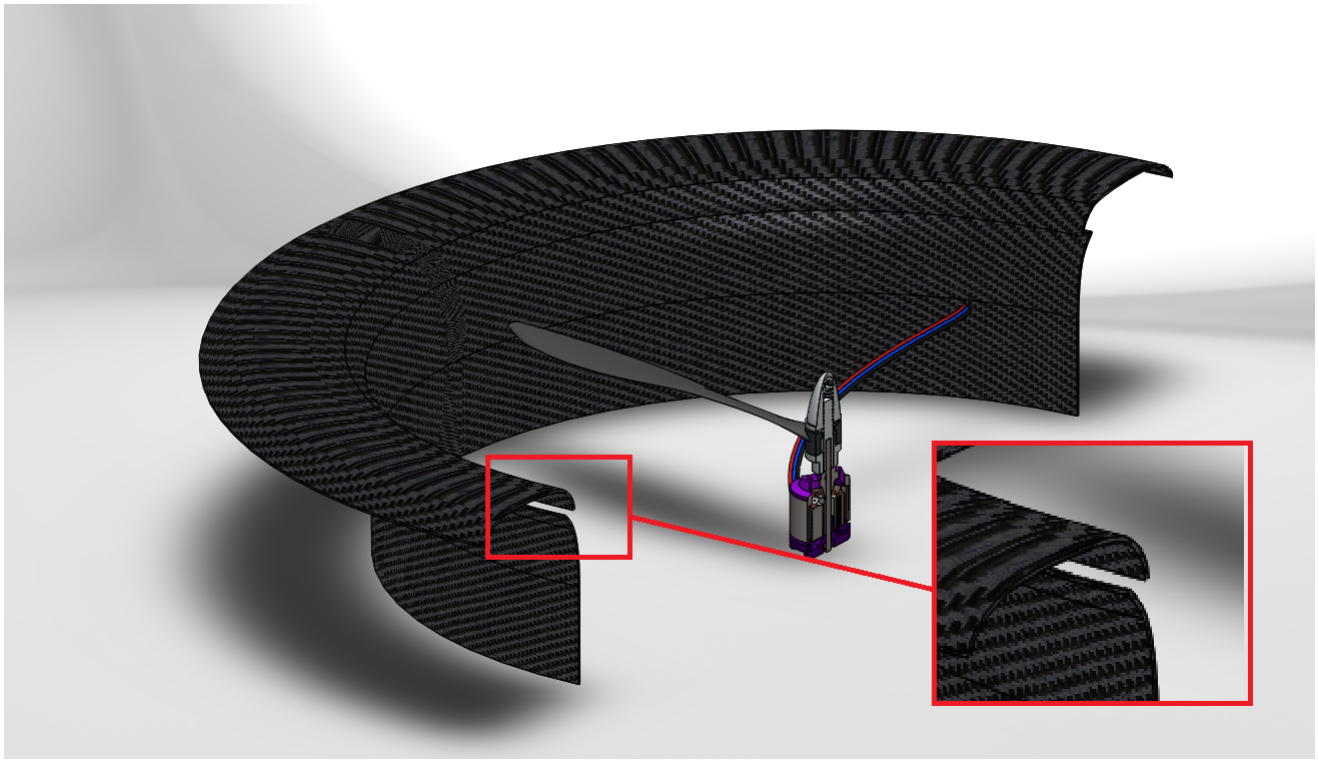

Figure 4.7: Cross Section View with Highlight of slotted flap on CAD Model

Due to the design of the annular wing, the flow is susceptible to separation as it flows into the duct, as shown in Figure 4.9. To counter this effect, a slot is located near the location of the separated flow. With the addition of the slot, fluid is able to enter the duct reducing flow separation, as can be seen in Figure 4.8. This leads to better flow control and reduced drag over the duct.

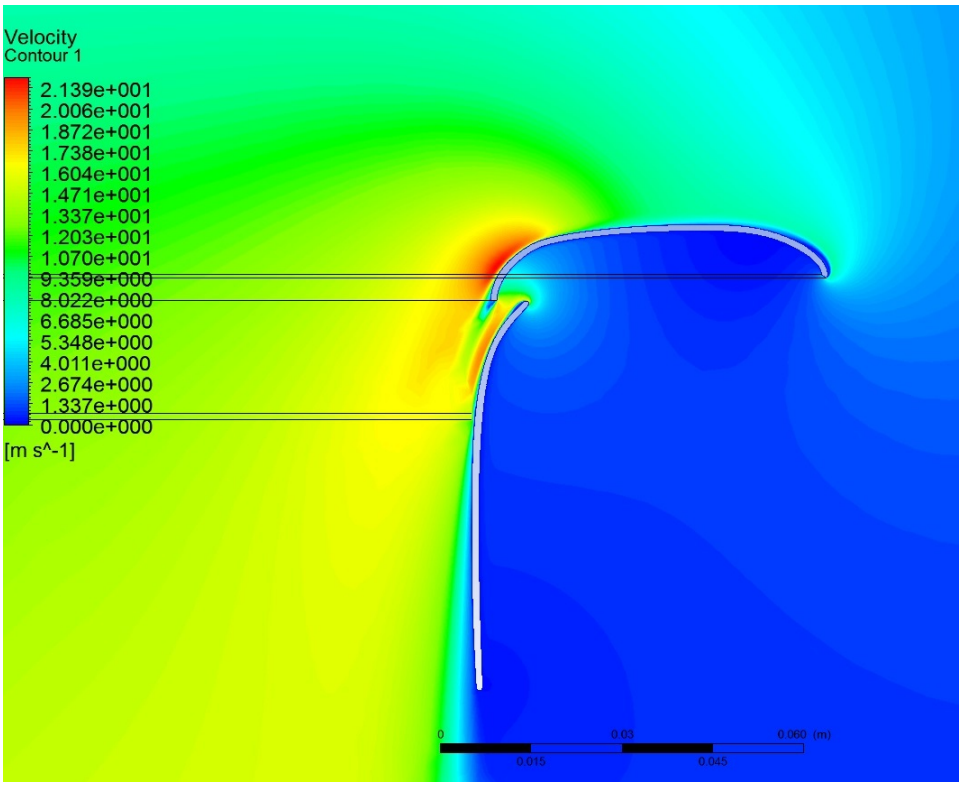

Figure 4.8: Cross Section View of Ducted Rotor with Boundary Layer Control

As shown in Figure 4.9, not having a slot at that location resulted in flow separation and poor flow and performance.

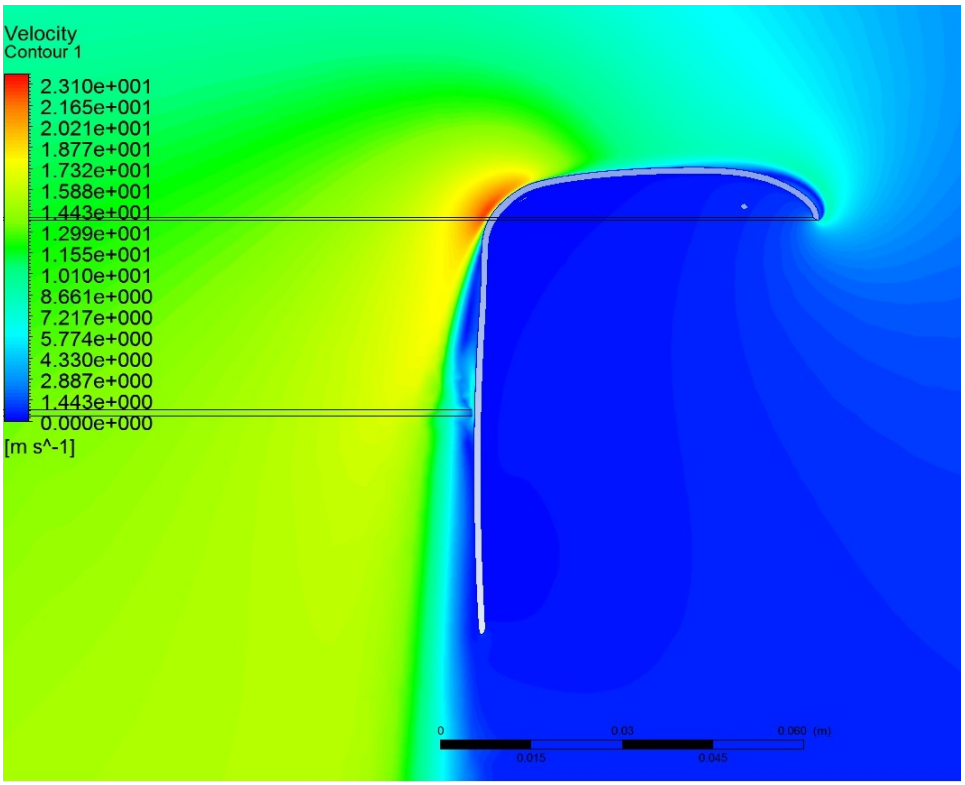

Figure 4.9: Cross Section View of Ducted Rotor without Boundary layer Control

4.2 Shroud

The shroud that contains the propeller benefits the design by increasing the aerodynamic performance of the propeller as well as acting as a physical barrier to increase safety.

The shroud increases the performance of the propeller by reducing flow vortices forming at the propeller tips. These vortices form due to the higher pressure below the propeller moving around the propeller tip to the lower pressure above. However, with the physical barrier of the duct, the flow vortices are prevented from forming. This results in a reduction of losses. A study by Martin and Tung showed that by minimising the clearance between the propeller tips and the shroud, the benefits are increased [16].

The CFD models and ducted rotor build for the physical tests were both designed to have a clearance of 1 mm. This clearance can be reduced further with more accurate construction methods.

4.3 Outlet Design

From Section 3.4, it was determined that the length of the duct will be approximately half of the throat diameter. Furthermore, earlier designs considered the benefits of diffusing the air flow as it left the duct. However, due to the increased complexity this would cause in the construction phase, the outlet of the duct was left at a design with straight sides. This benefited in the construction process as it only required a single piece mould for the ducted section, whereas a design with curvature would require a two piece mould.

4.4 Material

The duct was designed to be constructed out of carbon fibre. This was chosen due to its lightweight properties as well as its reduced surface roughness.

Chapter 5

Computational Fluid Dynamics

This chapter will identify the processes that were taken to implement the CFD simulations. It will also outline the steps that were taken to ensure their accuracy.

5.1 CAD

All computer-aided design (CAD) was completed using the Solidworks program. This allowed each design to be modelled accurately. Most of the physical components of this project were modelled using CAD as it allowed for a visual inspection of the component as well as having the high degree of accuracy that was required. Each iteration of the ducted rotor design was modelled in Solidworks in three dimensions, as required for the CFD processing. The required moulds for the duct wall and annular ring for the leading edge were also designed in Solidworks, which was then used by the UQ workshop to be cut from the CNC routing machine. The support that held the test rig to the ducted rotor was also modelled in Solidworks. This was then used to laser cut the acrylic. The test rig was also modelled in Solidworks for the visual inspection of its operation as well as acting as a guide during the construction process.

5.2 Meshing

The program Pointwise was used to complete all meshing requirements for the design process. This is due to its bottom up approach that allowed for easier meshing control on more complicated designs, such as the multi-element design in the ducted rotor. The automeshing feature in ANSYS CFX was not used because it was unable to acheive the quality that was required for this process. The other meshing program within ANSYS, which is ICEM, was not used because of the difficulties of getting a well-controlled mesh around the multi-element design, which is due to its

top down meshing approach.

The meshing approach implemented was the T-rex hybrid approach, which gave a better mesh structure to the unstructured tetrahedral at critical locations, such as the leading and trailing edges of the wing and duct. The benefit to the hybrid approach is that it allowed for the critical sections to have the high degree of structure that is required around the critical sections whilst allowing for more unstructured tetrahedral at less critical locations. This allowed for greater efficiency of time. The critical sections included the leading and trailing edge of both the duct wall and the annular ring.

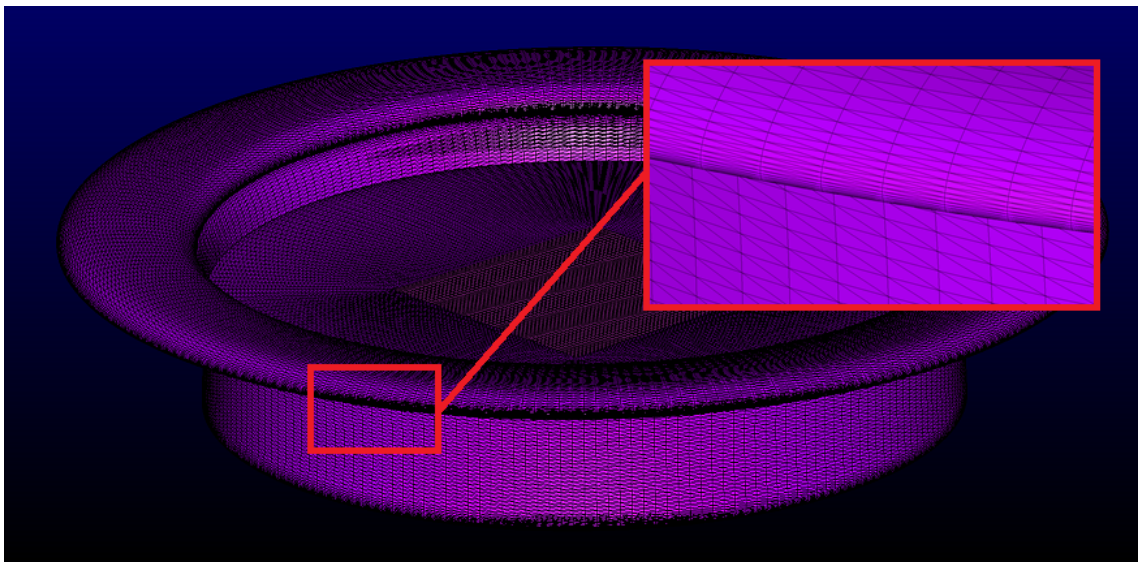

Figure 5.1: Mesh Structure Highlight

5.3 CFD

The CFD program used was ANSYS CFX in steady-state conditions. The method used in the simulation was using a finite thin disk, where the disk was used to simulate a momentum increase, such as a propeller would. The dimension of the disk had a depth of 1mm and a diameter of 304.8mm, which is the diameter of the propeller that the duct was designed for. This disk was then given a clearance of 1mm to the inner surface of the duct, which is also what the ducted rotor was designed to. For modelling of the turbulence, the Shear Stress Transport method was implemented due to its ability to better model flow separation and has been rated as the most accurate model for aerodynamic simulations[15]. The program was run in iterations until all residual values were below 1e-05 (See Figure 5.2) and all monitor points had converged onto a single value. The monitor points used in

the simulation were velocity measurements around the inlet and outlet of the ducted rotor.

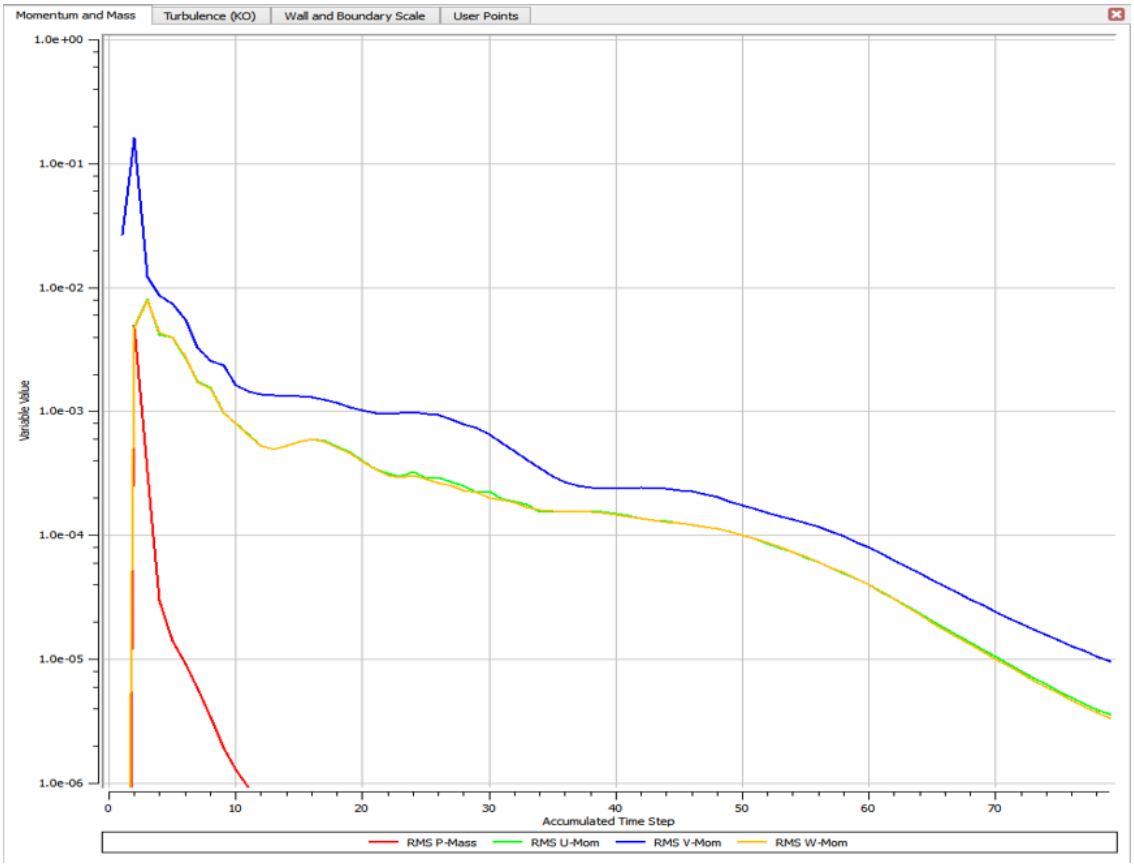

Figure 5.2: Residuals

Chapter 6

Construction and Test Apparatus

The ducted rotor was constructed for the purpose of carrying out physical tests to verify the CFD simulations and to prove the performance of the design.

Figure 6.1: Physical Ducted Rotor

6.1 Ducted Rotor Construction

The ducted rotor was constructed out of carbon fibre with acrylic supports, which was used to fasten the ducted rotor the test rig and electric motor.

6.1.1 Mould Construction

As required in the carbon fibre construction process, a mould for the ducted rotor was required. The mould was constructed out of plywood, which was machined by the UQ workshop using a CNC router. To get a high quality surface, the mould was sanded to get a smooth as possible surface. After this, the epoxy Araldite GY 191 and Aradur 2961 hardener was coated onto the surface with a mixture of microballoons, intended to seal the macro-porosity in the timber and to stop the

epoxy soaking into the mould during the curing process (As shown in Figure 6.2). A micro-porosity mould sealer was then used to improve the surface further. A release agent was then applied to the moulds five times to allow for easy removal of the product from the mould. The carbon fibre was vacuum bagged around the moulds and cured at room temperature.

Figure 6.2: Moulds

6.1.2 Material

The shroud and annular wing were both constructed out of carbon fibre for weight reduction. Two layers of 200 gsm plain weave carbon fibre was used for the annular wing whilst three layers was used for the shroud. These number of layers were decided after consultation with staff from the UQ composite group. The support struts were laser cut out of acrylic due to the required accuracy. The final mass of the shroud came to a total of 123 grams.

The test rig was constructed out of timber using a cantilever over a scale system (See Figure 6.3).

6.2 Test Apparatus

The test apparatus was constructed to use a cantilever design to measure the generated thrust on a load cell, as shown in Figure 6.3.

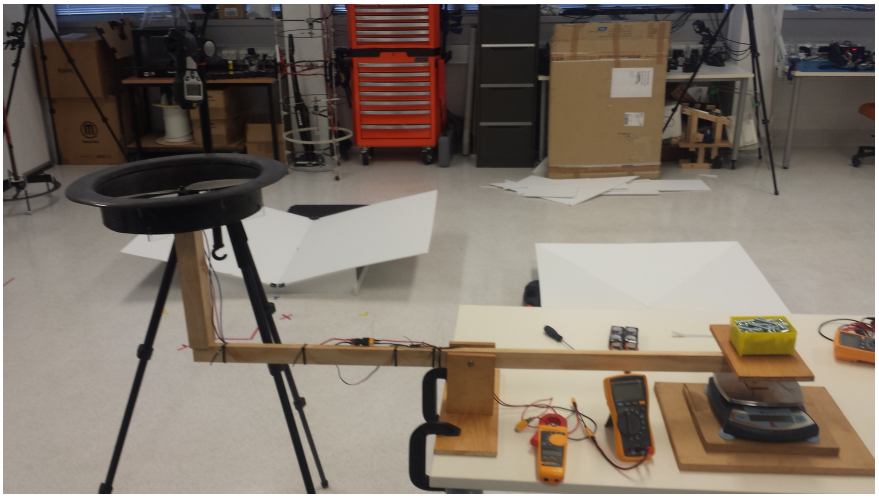

Figure 6.3: Test Apparatus

6.3 Methodology

The tests were conducted at multiple levels of throttle controls, starting at 90% throttle and decreasing by 10% increments. This allowed for a number of results at various levels of thrust and power consumption. Voltage, Current, RPM, and thrust results were recorded at each increment. The motor was given at least 10 minutes between each test to allow for adequate cooling of the electric motor. The battery was charged to full capacity between each test to allow for consistency. The ducted rotor and free propeller were both tested three times to ensure valid results were recorded.

The same tests were then conducted on a annulus wing to compare results. Further tests were then conducted on the duct without the annulus ring attached to for further comparison.

6.4 Hardware

6.4.1 Propeller

An APC 12 inch diameter propeller with a 4.7 inch pitch was used. This model was chosen due to high thrust capabilities at low RPM.

6.4.2 Motor

A 2836-9 880KV outrunner brushless motor with a maximum power rating of 243 Watts was used to drive the propeller.

6.4.3 Other Components

The items shown in Table 6.1 identify the other components that were necessary for the construction of the Ducted Rotor.

Table 6.1: Components

Component	Description
Carbon Fibre	200 gsm plain weave
Epoxy	Araldite GY 191
Hardener	Aradur 2961
ESC	20 Amp
Battery	3s
transmitter	Spektrum DX10t
Receiver	Spektrum

Chapter 7

Results and Discussion

This chapter reviews the results that were gathered from CFD simulations and physical testing.

7.1 CFD Results

CFD analysis was completed for the chosen design at multiple thrust values using the method mentioned in Section 5.3. Each separate simulation was run using different values of thrust generated by the simulated propeller. The results are shown in Figure 7.1 as well as numerically shown in Table 7.1. For each level of simulated propeller thrust, approximately 40% was developed from the shroud and annular wing combination. Although this seems significant, this does not translate into a 40% increase in total thrust. These results show that 40% of the thrust is developed by the aerodynamic contribution of the duct. This indicates that at the desired thrust levels, less of the load is applied to the propeller[9]. The decrease in load to the propeller contributes to an decrease in power consumption.

From the CFD simulations, expected power consumption was calculated by taking the total thrust and velocity through the simulated propeller by using Equation 7.1. It was assumed that the propeller in the ducted rotor would perform at maximum documented efficiency for the chosen propeller, which was 75%. The results are shown in Figure 7.2, which are used as the benchmark for the physical results.

$$P = \frac{FV}{\eta} \tag{7.1}$$

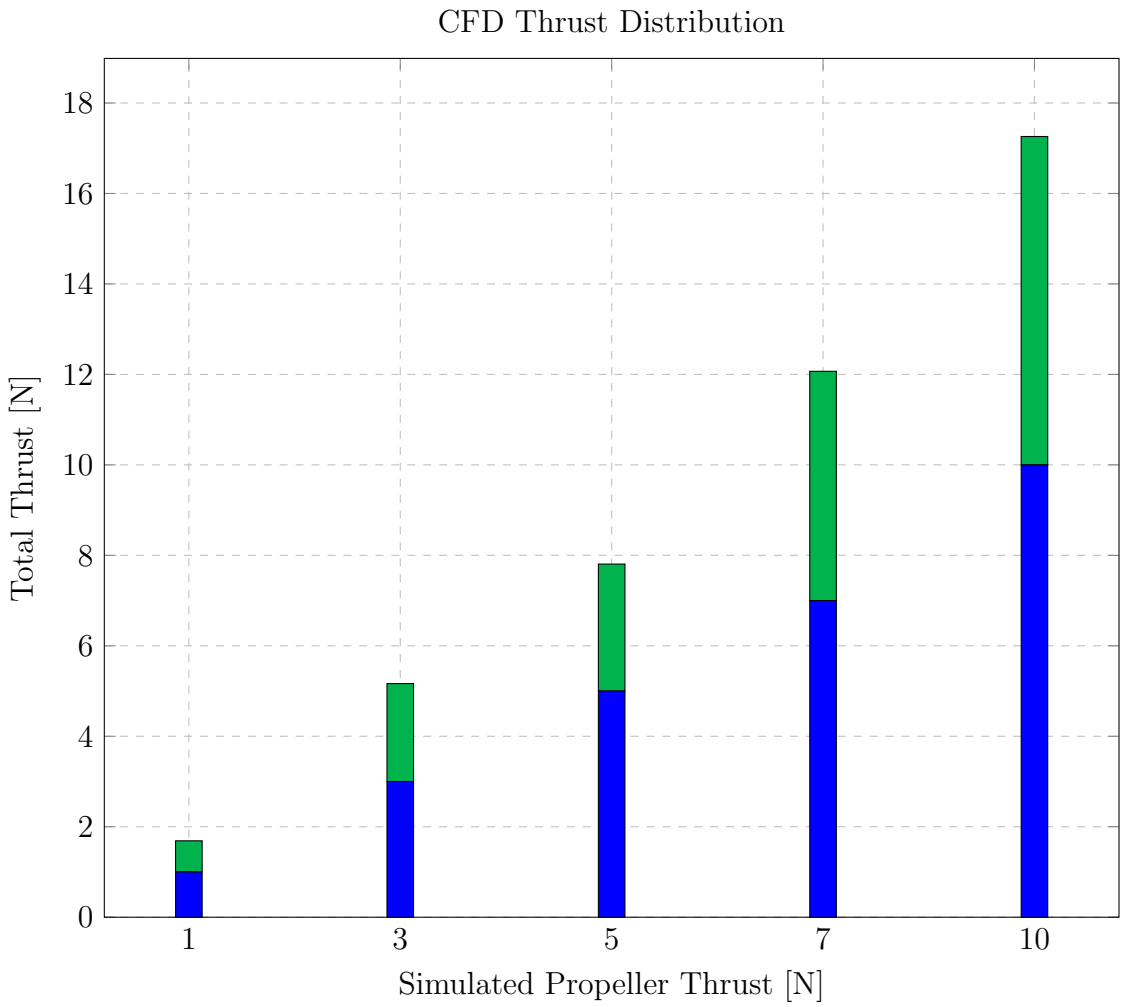

Figure 7.1: Thrust

Table 7.1: Thrust

Propeller Thrust [N]	Duct Thrust [N]	Total Thrust [N]	Percentage by Duct [%]
1	0.69	1.69	40.78
3	2.16	5.16	41.91
5	2.81	7.81	35.95
7	5.07	12.07	42.00
10	7.26	17.26	42.06

7.2 Static Thrust Results

Through both CFD simulations and physical experimentation, results were obtained that were able to compare the amount of thrust generated at given power consumptions, which are shown in Figure 7.2. The methodology for obtaining the results are outlined in Section 5.3 for the CFD simulations and Section 6.3 for the physical testing.

For hover conditions, the total weight of the design needed to be considered. Based on estimates, it was assumed that the total weight of the system will total 800 grams, which equates to 7.848 Newtons.

The results that are shown in Figure 7.2 compare the free propeller and ducted rotor for the given values of thrust and power consumption. The graph shows that the ducted rotor was able to consistently perform better than the free propeller. However, it also shows that the ducted rotor does not perform as well expected from the CFD simulations. The reason for these errors are explained in Section 7.6.

7.3 Power Efficiency

Due to the large number of results obtained through testing, it was possible to use linear interpolation to calculate the level of thrust for specific values of power consumption. The results shown in Table 7.2 indicate that at static thrust conditions, the ducted rotor performed better than the free propeller by reducing power consumption by 19.8%. These results are compared with the CFD modelling, which predicted a 34.9% reduction in power consumption.

Table 7.2: Static Thrust

	Free Propeller	Physical Shroud	Theory Shroud
Thrust (N)	7.848	7.848	7.848
Power Consumption (W)	145.76	119.50	102.45

7.4 Thrust Performance

Through further linear interpolation of the data, at the power consumption of 119.5 Watts, which is the power required for the physical ducted rotor at static conditions,

it can be seen that the ducted rotor generates an 11.7% increase in thrust than that of the free propeller. The CFD model was predicted to produce a 22.04% increase in thrust.

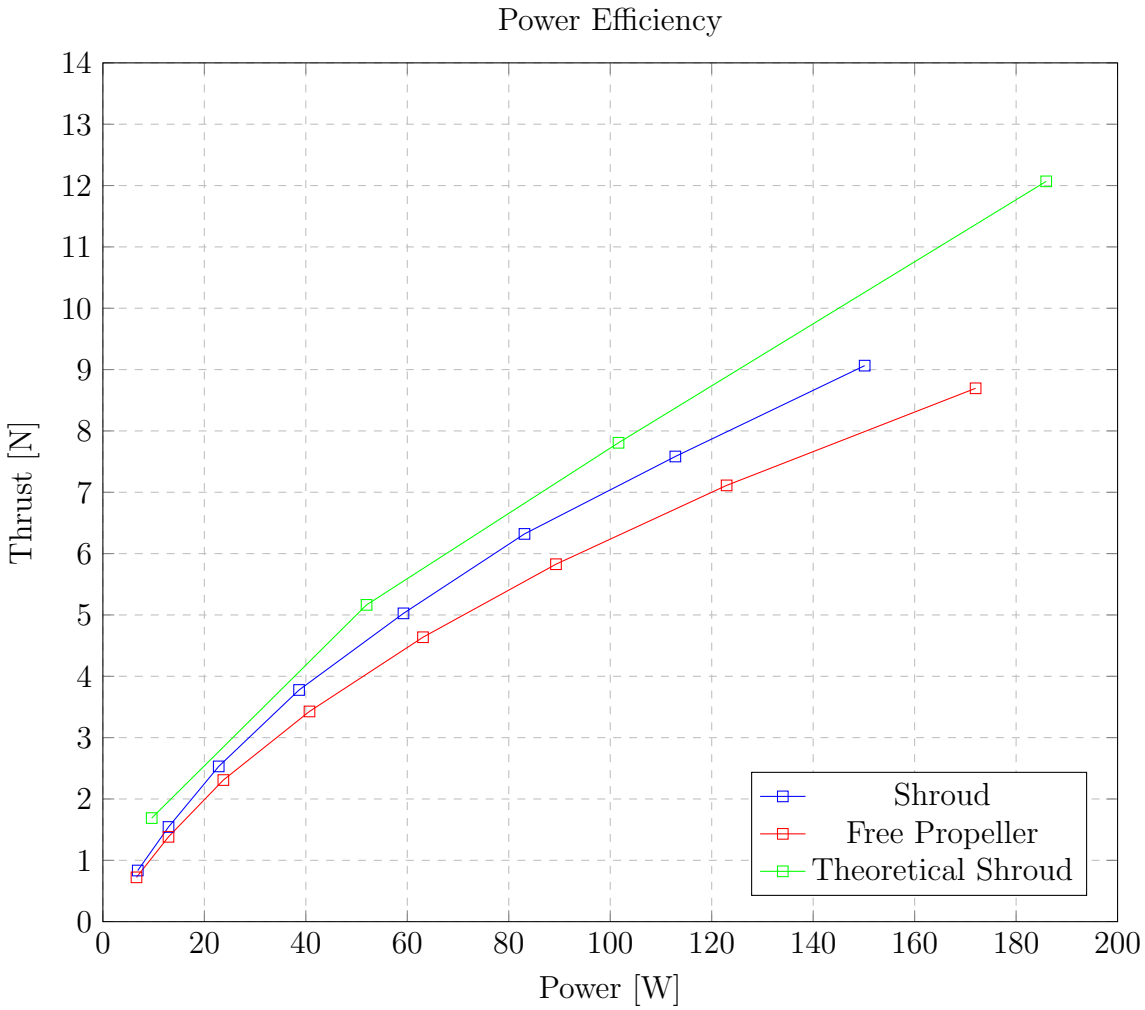

Figure 7.2: Power Efficiency

7.5 Further Testing

To compare the results that were recorded, a propeller within an annular ring and a propeller within just the duct design were also tested.

7.5.1 Foam Board Annular Ring

The foam board annular ring (Shown in Figure 7.3) was designed to have minimal clearance between the propeller and the ring, to mimic the benefits of reducing tip vortices around the propeller. The testing of the annular ring was designed to show how much of the benefits to the duct design were due to the shroud reducing

secondary flows, and how much thrust was produced by the duct. The results shown in Figure 7.4 indicate that the annular ring only produced a small benefit. However, this benefit may be smaller than expected due to the support struts that are underneath the annular ring but are present under the free propeller. However, from this data, it can be concluded that most of the benefit from the ducted rotor is from the leading edge design.

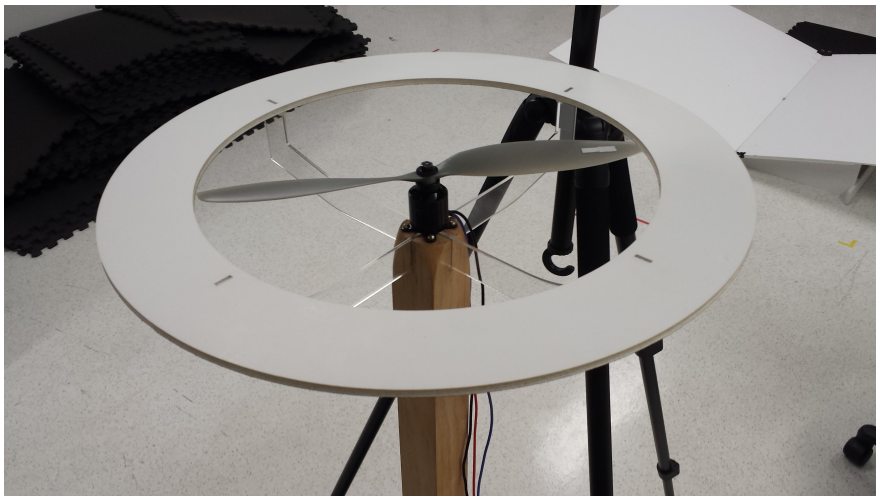

Figure 7.3: Foam Board Annular Ring

7.5.2 Duct without Annular Wing

A ducted rotor without the annular wing at the leading edge was tested. The results in Figure 7.4 show that the duct without the annular wing at the leading edge performed worse than the free propeller. This was expected as this confirms that the flow would separate from the duct without the leading edge design, causing massive losses within the system.

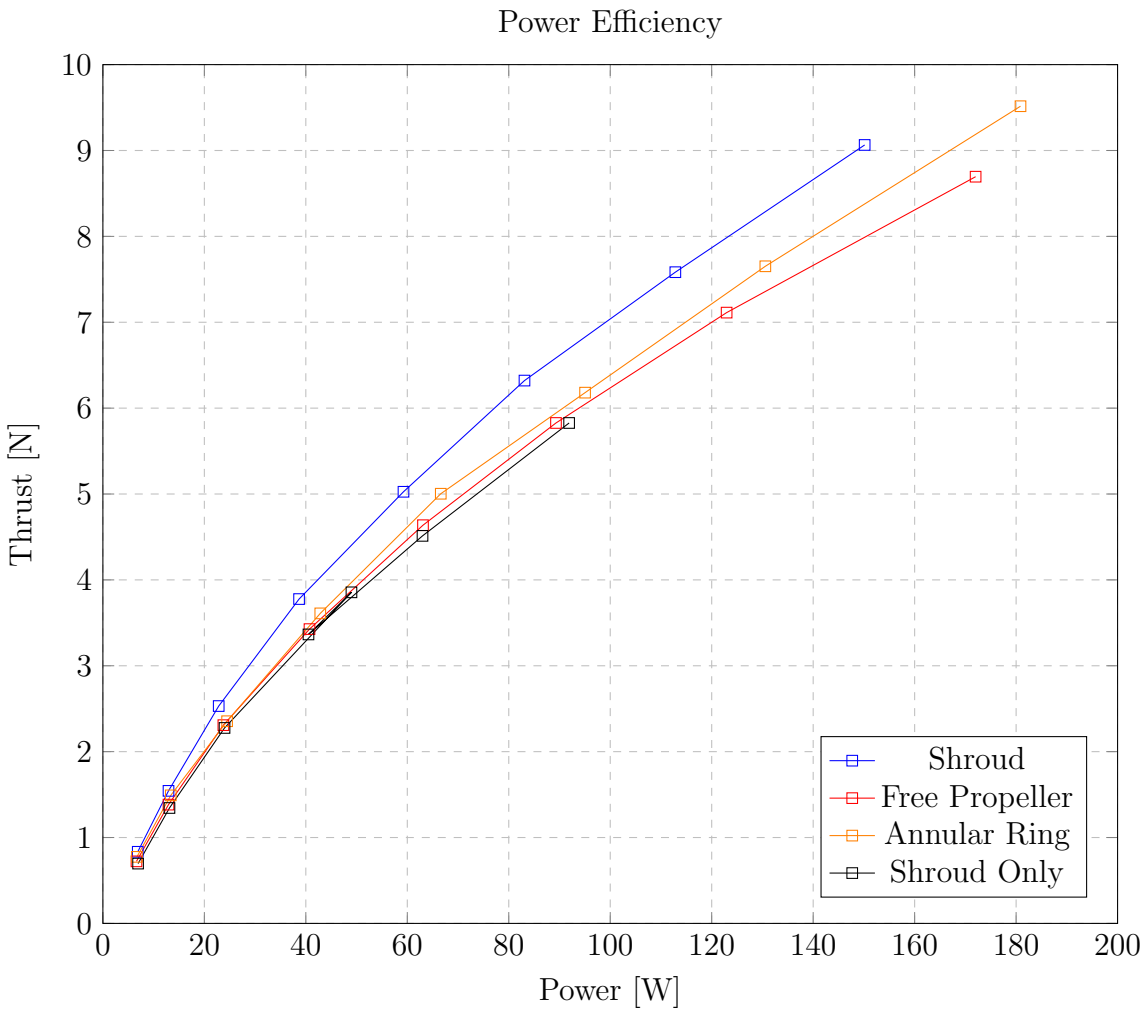

Figure 7.4: Comparison with Further Testing

7.6 Error Analysis

Throughout the simulations and physical testing, it should be noted that a number of factors can cause discrepancies in the results, as noted:

- CFD finite actuator disk method does not consider the swirl generated by a propeller
- The CFD model did not consider the impacts that the physical presence of the test right would have had on the physical results
- The CFD model did not consider the impact of the motor and support within the simulation
- The surface of the ducted rotor tested was not ideal, and further improvements can be made on it

Overall, at the hover conditions, which was a desired thrust of 800 grams, the error between the CFD model and physical testing is 16.64%. At the given power consumption of 119.5 Watts, the error between the CFD modelling and thrust is 9.90%. Through further refinement of the physical testing, it is believed that these errors can be reduced further.However, these errors are considered to be reasonable and this shows that the physical testing was able to confirm the CFD results.

Chapter 8

Conclusions

8.1 Summary and conclusions

In summary, the defining aims of the thesis were achieved and the innovative features used in this design were shown to be effective in increasing the performance of a rotor. The ducted rotor design showed considerable improvements in performance, with an overall decrease in power consumption of 19.8% Furthermore, the theoretical CFD model provided accurate results with a maximum margin of error of 16.64% between the physical tests and the CFD models.

The upper camber at the leading edge of the annular wing was determined to be critical in the reduction of flow separation. Through analysis it was found that the annular wing around the leading edge required a certain level of camber to minimise flow separation as the fluid flows over the leading edge into the duct.

The annular wing was determined to have an optimal chord length of 55 mm, thereby producing a planform area that was large enough to produce a significant amount of thrust without being compromised by the skin friction losses.

A slotted flap design, was shown to be effective at reducing flow separation as the fluid flows into the duct. This slotted flap design is important for the reduction of losses. The incorporation of the slot leads to better flow control and a reduction in drag over the duct.

The shroud containing the propeller benefits the design of the ducted rotor by reducing the secondary flows that form at the tips of the propeller. This was possible due to the minimised clearance of only 1 mm between the shroud and the propeller.

The physical presence of the shroud was also beneficial to the safety of the design.

8.2 Possible future work

There are various aspects that could be considered for possible future work on the duct design. First of all, it is believed that the current design can be improved upon by improving the surface quality of the carbon fibre, as well as using thinner support structures to replace the current 2 mm thick acrylic. With a revised construction method, it is believed that the ducted rotor will be able to have finer tolerances, reducing the clearance between the shroud and the propeller tips. Further improvements may also be achieved by designing the outlet so that it may diffuse the flow, to reduce any unwanted flow distortions. Finally, it is also possible that a similar analysis on the leading edge of the shroud might lead to further performance increases. This would mean that a beneficial pressure distribution would be placed on two leading edges, instead of just one.

References

[1] S. N. Air and S. Museum. (1998). Hiller model 1031-a-1 flying platform, [Online]. Available: http://airandspace.si.edu/ (visited on 09/11/2015).

[2] F. Global. (1967). Flight global archive, [Online]. Available: http://www.flightglobal.com/ (visited on 09/11/2015).

[3] M. J. Company. (2013). Martin jetpack, [Online]. Available: http://www.martinjetpack.com/ (visited on 09/11/2015).

[4] Honeywell. (2015). T-hawk mav, [Online]. Available: https://aerospace.honeywell.com/thawk (visited on 09/11/2015).

[5] R. Walker, "Design, construction and control of a ducted rotor-in-ground-effect micro air vehicle," University of Queensland.

[6] A. Wallis, *Axial flow fans and ducts*. Brisbane: John Wiley and Sons, 1983.

[7] J. Anderson, *Introduction to Flight*. New York: McGraw Hill, 2012.

[8] F. White, *Fluid Mechanics*. New York: McGraw Hill, 2011.

[9] B. W. McCormick, *Aerodynamics of V/STOL Flight*. Toronto, Ontario: General Publishing Company, 1999.

[10] J. Pereira, "Hover and wind tunnel testing of shrouded rotors for improved micro air vehicle design," PhD thesis, University of Maryland, 2008.

[11] S. R and S. Dinavahi. (2011). Shape optimization of a ducted rotor system for aerodynamic performance.

[12] Prabhakar and J. Ohri. (2013). Cfd analysis on mav naca 2414 wing in high lift take off configuration for enhanced lift generation.

[13] B. W. D. Foster H. Irwin, *The two-dimensional flow around a slotted flap*. Farnborough: Aerodyanmics Dept. RAE, 1971.

[14] R. B. N. Abuaf and C.Lee. (1997). Effects of surface roughness on heat transfer and aerodynamic performance of turbine airfoils.

[15] ANSYS. (2015). Innovative turbulence modeling, [Online]. Available: http://www.ansys.com/staticassets/ansys/staticassets/resourcelibrary/techbrief/cfx-sst.pdf (visited on 09/11/2015).

[16] P. Martin and C. Tung. (2004). Performance and flowfield measurements on a 10-inch ducted rotor vtol uav, [Online]. Available: http://rotorcraft.arc.nasa.gov/publications/files/Martin_2004.pdf (visited on 08/08/2015).